The Astronomical Journal, 139:2308–2318, 2010 June doi:10.1088/0004-6256/139/6/2308
© 2010. The American Astronomical Society. All rights reserved. Printed in the U.S.A.

SEPARATED FRINGE PACKET OBSERVATIONS WITH THE CHARA ARRAY. I. METHODS AND NEW ORBITS FOR χ DRACONIS, HD 184467, AND HD 198084

C. D. Farrington[1], T. A. ten Brummelaar[1], B. D. Mason[2], W. I. Hartkopf[2], H. A. McAlister[3], D. Raghavan[3], N. H. Turner[1], L. Sturmann[1], J. Sturmann[1], and S. T. Ridgway[4]

[1] The CHARA Array, Mt. Wilson Observatory, Mt. Wilson, CA 91023, USA; farrington@chara-array.org, theo@chara-array.org, nils@chara-array.org, sturmann@chara-array.org, judit@chara-array.org

[2] US Naval Observatory, 3450 Massachusetts Avenue NW, Washington, DC 20392-5420, USA; bdm@usno.navy.mil, wih@usno.navy.mil

[3] Center for High Angular Resolution Astronomy, Georgia State University, P.O. Box 3969, Atlanta, GA 30302-3969, USA; hal@chara.gsu.edu, raghavan@chara.gsu.edu

[4] National Optical Astronomy Observatory, P.O. Box 26732, Tucson, AZ 85726-6732, USA; sridgway@noao.edu

Received 2009 October 15; accepted 2010 March 28; published 2010 April 22

ABSTRACT

We present the modification of the orbits of χ Draconis and HD 184467, and a completely new orbit for HD 198084, including data taken at the Center for High Angular Resolution Astronomy (CHARA) Array. These data were obtained using a modification of the technique of separated fringe packets (SFPs). The accuracy of the SFP data surpasses that of data taken by speckle, but the technique is much more time and labor intensive. Additionally, using SFPs with the CHARA Array, it is possible to obtain separations below the detection range of speckle interferometry ($\geqslant$30 mas) above the range in "classic" long-baseline interferometry where fringes from a binary overlap are no longer separated ($\leqslant$10 mas). Using spectroscopic binary systems with published speckle orbits, we are able to test our new measurements against their ephemerides to calibrate the method as well as produce entirely new orbits for systems with no current astrometric observations.

Key words: binaries: close – infrared: stars – stars: individual (chi Draconis, HD 184467, HD 198084) – techniques: high angular resolution – techniques: interferometric

1. INTRODUCTION

The Center for High Angular Resolution Astronomy (CHARA) Array (ten Brummelaar et al. 2005) is well suited for observing binaries with angular separations in the submilliarcsecond regime using the traditional interferometric visibility method (Boden et al. 1999). Another approach (Dyck et al. 1995; Lane & Muterspaugh 2004; Bagnuolo et al. 2006) applies to stellar systems where the components of a binary are sufficiently far apart in projected angular separation that their fringe packets do not overlap and the visibility fitting approach is not relevant. When observed with optical long-baseline interferometers (OLBI), these separated fringe packet (SFP) binaries extend out into the regime of systems resolvable by speckle interferometry at single, large-aperture telescopes and can provide additional measurements for preliminary orbits lacking good phase coverage, help constrain elements of already established orbits, and locate new binaries in the undersampled regime between the bounds of spectroscopic surveys and speckle interferometry. In this process, a visibility calibration star is not needed, and the SFPs can provide an accurate vector separation. In this discussion, we apply the SFP approach using the CHARA Array's "Classic" beam combiner to χ Draconis and HD 184467, for which visual and spectroscopic orbits exist, to show the method properly determines the correct positions, and to HD 198084, a previously unresolved spectroscopic binary.

2. PREVIOUS SFP APPLICATIONS

In order to determine the correct orientation for a secondary source with an interferometer, there is a potential ambiguity of 180° in position angle that needs to be overcome. Methods for removing this ambiguity include the use of closure phase with three or more telescopes (Shao & Colavita 1992), as well as the dispersed fringe technique with two telescopes where fringes are spectrally dispersed within their bandpass (Schloerb 1990). The technique applied here uses two baselines in different orientations: either two pairs of telescopes used simultaneously or one pair used two or more times during a night as the Earth rotation changes the pair's orientation relative to the baseline of the telescope pair. The location of the secondary star can then be extracted using simple geometric techniques, bypassing visibility measurements completely. This method, which has been rarely used since the advent of OLBI, can now be fully tested and applied to current and future multiple star studies.

In order to validate the transfer scan mode for the Fine Guidance Sensors on the *Hubble Space Telescope* in the early 1990's, Franz et al. (1992) conducted a series of tests on binary stars in the Hyades cluster using the transfer functions, which are plots of the visibility of the interference pattern of the two beams of linearly polarized light. As the polarizations of these beams are orthogonal, the transfer functions represent sensitivities in the x and y directions. At the time, the program did not have a suitable list of calibrators with which to determine the absolute directions of x and y with respect to known sources, so it was impossible to completely determine with high accuracy the absolute locations of the possible companions.

Dyck et al. (1995) conducted similar experiments using the Infrared Optical Telescope Array (IOTA) on the well-studied, widely separated binary ζ Hercules, in an attempt to revive the notion of using a two-telescope interferometer to bypass the position angle ambiguity associated with classical interferometry. The practical usage and theory on the application of this process provided the basis for SFP investigations as applied in this project. Nearly a decade passed after Dyck et al. (1995) published this groundwork before another example of SFP study was put into practice. Lane & Muterspaugh (2004) used a fringe tracker on the Palomar Testbed Interferometer

(PTI) to allow for delay scanning on a larger angular scale while keeping the phase information for differential astrometry of a binary system. During the scientific commissioning of the CHARA Array, Bagnuolo et al. (2006) completed a similar study of separated fringes using a slightly different technique on 12 Persei, a less widely separated binary with a previously published speckle orbit.

2.1. SFPs with IOTA

As noted by Dyck et al. (1995), for a binary star for which both components are within the field of view of the interferometer, it is possible that given the correct orientation, the interferometer will produce non-overlapping fringes for each star at widely separated delay positions. The observed double interference pattern can be seen as a linear combination of the individual fringes, scaled by the relative brightness and the extent of resolution (angular diameter) of each source. The difference in delay or path between the two fringe packets is based upon the orientation of the binary system (separation and position angle) and the orientation projected onto the sky of the baseline in use at the time of the observation and modified by atmospheric seeing variations—mostly from the movement of fringes during measurement due to differing air path lengths referred to as "piston error." In the case of binaries with small separations or orientations where the baseline is nearly orthogonal to the separation of the system, the fringe patterns will overlap and the standard visibility analysis is applicable. For wider binaries, each star will produce a distinct interference fringe of its own, with relative amplitudes proportional to the brightness of the individual sources and the degree to which the stellar photospheres are resolved.

For IOTA, it was possible to drive the delay line at a high enough rate to record the delay referenced positions of each fringe packet, "freeze" the phase-perturbing effects of the atmosphere, and obtain a snapshot of the one-dimensional cross section of the system. This technique, called "delay referencing" by Dyck et al. (1995), allows for the referencing of different source components to a common fiducial and preserves the relative positional information of the system. This was then tested on ζ Her using the north–south IOTA baseline on multiple occasions, alternating between ζ Her and a single unresolved calibrator star to show that the formation of the secondary fringe packet was not due to instrumental artifacts. Additionally, modeling with synthetic data was done to determine how well these "snapshots" could handle multiple components. Using a system comprised of four components, the theoretical response of IOTA on both baselines was calculated with varying separations and brightness ratios, and it was determined that the best course for observing systems with multiple components would be to observe the source over a wide range of times and allow the rotation of the projected baseline to help sample the (u, v) plane. Dyck et al. (1995) have conclusively shown that this technique was able to locate and measure the relative position of the secondary with reasonable accuracy on separations available to IOTA, and their work provides the foundation for the SFP survey at the CHARA Array.

2.2. Previous SFPs with PTI and the CHARA Array

Nearly a decade later, two efforts (Lane & Muterspaugh 2004; Bagnuolo et al. 2006) used similar approaches to approximately obtain the same information. Through the use of a fringe tracker on PTI on the "wide" binary HD 171779, Lane & Muterspaugh (2004) were able to obtain separation errors of $\approx$16 μas. As each 150 μm delay modulated scan was typically 1.5 s and the fringe separation nearly one-third of the scan, the phase locking fringe tracker was absolutely necessary to keep the positional and temporal coherence of the individual fringes intact. Using a different, yet complementary approach of "side-lobe verniering," the modulation of the separation as the secondary's fringe packet rides over the side-lobes of the primary, Bagnuolo et al. (2006) produced separation errors of $\sim$25 μas for 12 Per with a significantly smaller separation ($\sim$50 mas from CHARA versus $\sim$250 mas from PTI). The "free" phase reference from the modulation of separation from the side-lobes provided the CHARA Array, a method to obtain excellent accuracy for smaller angular separations without using a fringe tracker. Moreover, the accuracy of the side-lobe verniering provided a refinement of an existing visual and spectroscopic orbit and yielded the fundamental parameters of the system to an accuracy of $\sim$1%. Both of these determinations show the limiting accuracy of single baseline measurements with phase referencing on their respective instruments but require significant observing time dedicated to a single object due to the slow rotation of the baseline projection.

3. CHARACTERIZING SFPs

OLBI observations of SFP binaries resemble lunar occultation measurements in that they are one-dimensional scans across a system that sample a projected angular separation between the primary and secondary components. The limiting resolution of the CHARA Array can be defined by the location of the first null in the fringe visibility, and is computed to be 1.6 mas, with the CHARA Array's K' filter ($\lambda_0 = 2.1329$ μm, $\Delta\lambda = 0.3489$ μm) on the longest baseline available (S1-E1 $\sim$330 m). Higher resolutions are available by measuring the visibility higher up the visibility curve, but for SFP measurements we shall be examining a different regime that does not require visibility calibrations. Our experience shows that for systems with components of nearly equal magnitudes, we can reasonably detect SFPs separated by the coherence length of an interferometric observation, a quantity determined by the spectral bandpass employed. One such example is the short-period spectroscopic binary HD 4676, for which data were taken in late 2005. The pair had a maximum elongation of approximately 10 mas and clearly exhibited a secondary packet, as shown in Figure 1. In this context, the range of projected separations being sampled is bounded by the maximum range of delay of the scanning dither mirror (142.43 μm) for the "wide" case and the coherence length

$$\Lambda_{\rm coh} = \frac{\lambda_0^2}{\Delta\lambda}, \quad (1)$$

where λ_0 is the central wavelength of the filter used, $\Delta\lambda$ is the effective filter width and $\Lambda_{\rm coh}$ is a measure of the width of the fringe packet. This quantity is solely defined by the filter in use and is calculated to be 13.04 μm for the K'-band filter used for these data. The instantaneous projected baseline is based on the relation:

$$\vec{B} = \sqrt{u^2 + v^2}, \quad (2)$$

where u and v, the snapshot projection of the baseline in spatial frequency units (cycles arcsec^{-1}; cf. Dyck 2000), are defined by

$$u = [B_E \cos h - B_N \sin b \sin h + B_L \cos b \sin h]/(206265\lambda) \quad (3)$$

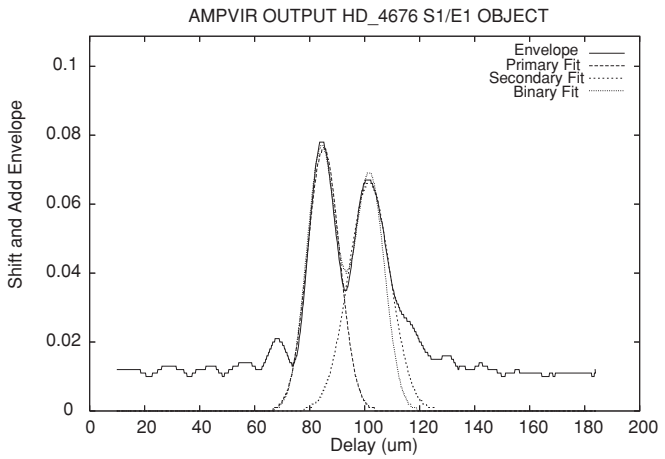

Figure 1. Fringe envelope for HD 4676. Taken 2005 October 7 on the S1-E1 baseline at maximum elongation. While side-lobes can introduce large errors in calculating separation from data such as this, it is still easily discernable at this (≈10 mas) separation.

and

$$v = [B_E \sin\delta \sin h + B_N(\sin b \sin\delta \cos h + \cos b \cos\delta) - B_L(\cos b \sin\delta \cos h - \sin b \cos\delta)]/(206265\lambda). \quad (4)$$

Here B_E, B_N, and B_L are the position vectors of each telescope with respect to the reference telescope S1, h and δ are the hour angle and declination of the object, b is the latitude of the observatory, and $\vec{B}$ is the instantaneous projected baseline length. This relation, along with the range of motion of the dither mirror, allows us to determine the one-dimensional "field of view" of the instrument for searching outside of the primary fringe packet using

$$\vec{\rho}_{\rm mas} = \frac{206.265\vec{\rho}_{\mu\rm m}}{B(m)}. \quad (5)$$

4. MAGNITUDE AND MAGNITUDE DIFFERENCE LIMITATIONS

The CHARA Array splits the starlight at 1 μm using a dichroic sending the shorter wavelength light to be used for tip-tilt tracking of the star and longer wavelengths to the CHARA IR camera where the K' band is used for fringe measurements. This imposes two magnitude limits for targets that can be observed. Locking onto an object using the CHARA tracking servo is the first limit and has the greatest sensitivity so it is the least important restriction for this project. Currently, the CHARA Array is able to maintain tracking on systems down to $V = +10.5$.

In order to transport the light to the CHARA Beam Combination Laboratory, a non-trivial number of reflections is needed, and through the 19 reflections from the telescope to injection into the "Classic" beam combiner, a significant amount of light is lost. This, combined with the camera sensitivity in the slowest read mode (250 Hz), limits the magnitudes available in the science bands (K, H, and J). The current observational limit for the CHARA Array is +8.5 using the K' filter.

Two factors influence detection of the secondary fringe. It becomes increasingly difficult to quantify the location of the secondary fringe as the separation decreases. Figure 2 shows the effect of Δm and separation variations on SFP measurements.

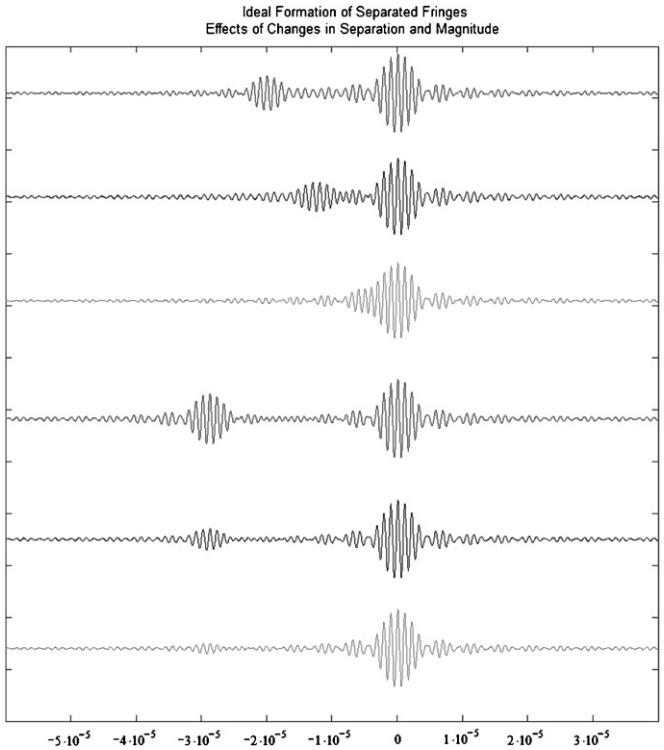

Figure 2. Effects of Δm and separation on separated fringe packets. The top three scans show the effects of decreasing separation on a $\Delta m = 1.0$ set of fringes. It is easy to see how, as the separation decreases, the discernability of the location of the secondary fringe becomes increasingly more difficult. The bottom three scans show increasing Δm of 0.5, 1.5, and 2.5 mag with a constant separation. Below $\Delta m = 2.0$, it becomes a non-trivial matter to locate the secondary even under ideal (no noise) conditions which can be corrected for to some extent by the summation of multiple scans to increase the signal-to-noise ratio.

As seen in the bottom three panels, the fringe contrast changes from clearly visible with $\Delta m = 0.5$ at the top, $\Delta m = 1.5$ in the middle, to barely discernable at a $\Delta m = 2.5$ at the bottom. These ideal noiseless fringes are relatively easy to see. For realistic cases, the secondary fringe packet can be unseen for individual scans, but discernable as the envelope function of the scans are integrated in a shift-and-add process. For systems where the companion is faint, increasing the number of scans for each data set can increase the chances of detecting a companion with a large magnitude difference. The maximum Δm we can reasonably obtain from the CHARA Array in the described mode is approximately $\Delta m = 2.5$.

Using the differential resolution to our advantage, and as long as the companion is within the magnitude limit of the detector, it should be possible to detect the secondary fringe with a larger magnitude difference than the one shown in Figure 2 as the larger star is progressively resolved. Instead of measuring the magnitude ratio directly, we obtain the visibility ratio of the two fringes and if both components are unresolved, the ratio of the amplitudes of the fringes will provide a measure of the magnitude ratio. If the smaller star is essentially unresolved and the larger has some degree of resolution, the companion's visibility should remain constant while the larger star's visibility decreases as the baseline increases providing a means to measure the magnitude limit beyond the described Δm limitations above with the help of the decreasing visibility ratio. These same systems also have a smaller differential magnitude in the observed K band due to increasing sensitivity for faint companions which increases the benefit for secondaries which have a larger V-band magnitude difference.

At this point, it is worth mentioning a special case that can reintroduce the 180° ambiguity inherent in one-dimensional interferometric observations and is directly related to one of the objects discussed here. The primary star of a system is considered to be the most massive and often the brightest. Such systems will produce two fringe packets where identifying the primary is simple. A subset of binary systems contain both an evolved and an unevolved component, where the evolved may be the brighter of the two components and is much larger than its companion. This type of system can confuse the fringe selection as many of these larger stars become resolved on the long baselines required to provide separate fringe packets for the two components. Observing these systems on the long baselines produces a fringe packet for the larger star that is partially or even fully resolved and decreases the fringe amplitude of the primary packet so that it is often smaller than its less resolved and dimmer companion. This effect can be seen in the observations of χ Draconis, a large F8IV-V primary with a late-G/early-K dwarf secondary.

5. TEMPORAL COHERENCE

The largest source of error for the determination of the separation between SFPs is temporal coherence, which encompasses the fringe movement during the scan. Also called "piston error," quantifying this is considerably more difficult than the previously discussed error sources. Using Equation (6) from Lane & Muterspaugh (2004) with some modifications based on the different instrument and recording times and eliminating the term relating to the phase tracker available at PTI, the expression is then given by

$$\sigma_{tc}^2(\mathrm{mas}) = \left(\frac{\lambda}{2\pi B}\right)^2 \frac{1}{N} \int_0^\infty A(f) S(f)\, df, \tag{6}$$

where N is the number of scans in a data set and $A(f)$ is a measure of the power spectral density of fringe phase observed through the atmosphere and is approximated by

$$A(f) = f^{-\alpha}. \tag{7}$$

The α parameter is within the range 2.5–2.7. $S(f)$ is the sampling function representing the phase sampling while scanning across one fringe and the time taken to move between fringes given by

$$S(f) = \sin^2(2\pi f \tau_p)\mathrm{sinc}^2(\pi f \tau_\Lambda). \tag{8}$$

Here, τ_p is the time delay between recording of individual fringes (fringe separation (Δd)/scan velocity (v_s)), and τ_Λ is the time required to scan the individual fringes (coherence length (Λ)/scan velocity). We obtain a value for σ_{tc} comparable with the estimate given by Lane & Muterspaugh (2004) for a system without a fringe tracker (0.491 mas versus 0.016 mas) using the parameters for the CHARA Array ($B = 300$ m, $\lambda = 2.15$ μm, $N = 220$ scans, $\alpha = 2.5$, $v_s = 569.7$ μm s^{-1}, $\Delta d = 60$ μm, and $\Lambda = 13.04$ μm). Compared to the previous error terms, this is by far the dominant error term for the measurement of separated fringes for the CHARA Array.

6. ADDITIONAL ERROR SOURCES

Other instrumental factors can influence the determination of accurate separations between fringes, but are mostly neglected as they are orders of magnitude smaller than the largest error source. For the calibration of the separation of the fringes, it is necessary to know the location of the dithering mirror to high precision. Fortunately, the mirror position is known to 0.1 μm, which is less than 0.1 mas on the longest baselines when all other quantities are known.

In order to accurately measure the position of a star's fringes, the length of the baseline must also be known to very high precision, which in turn implies high precision measurements of the locations of the telescopes. The location of each telescope and incremental delay mirror are known to approximately a millimeter, so when converting the separation of fringes from microns in the lab to separation on the sky, the uncertainty of the baseline values produces errors many orders of magnitude smaller than all other sources of error discussed here. Additionally, the errors involved in this process only shift the offset of the fringe locations and speed at which they drift, which does not significantly affect measurement of the fringes.

6.1. Data Reduction

The SFP data are de-biased and corrected for background and imbalances in light intensities from the two telescopes in the same way as the visibility amplitude data reduction described in ten Brummelaar et al. (2005). Essentially, the fringe signal is the difference in intensity measured on either side of a beam splitter normalized by the total intensity. We write the fringe signal as $F(p)$, where p is the position of the dither mirror in microns and the fringe signal F is a dimensionless quantity. In order to locate the fringes, we need to calculate the fringe envelope, i.e., we must demodulate the fringe and find the analytic signal as defined by Bracewell (2000).

We begin by calculating the Fourier transform of the fringe signal

$$f(k) = \int F(p) \exp^{-i2\pi kp}\, dp, \tag{9}$$

and then impose a windowing function on the inverse transform

$$E(p) = \int w(k) f(k) \exp^{i2\pi kp}\, dk, \tag{10}$$

where

$$w(k) = \begin{cases} 1, & k_1 < k < k_2 \\ 0, & \text{otherwise.} \end{cases} \tag{11}$$

The frequencies k_1 and k_2 form a bandpass around the spatial frequency of the fringes. The result is a complex function whose modulus is the fringe envelope function

$$e(p) = |E(p)|. \tag{12}$$

In the extremely high signal-to-noise case, this envelope function should be the shape of the power spectrum of the filter used, nominally a sinc function. However, due to piston errors and fringe drift, these peaks more often resemble a Gaussian. In order to locate the center of the two peaks and find the separation of the two fringe packets, we therefore fit a Gaussian shaped curve to each peak. An example demodulated fringe envelope function is shown in Figure 1.

7. OBSERVATIONS

The three objects chosen as test cases for this method were taken from the CHARA Catalog of Orbital Elements of Spectroscopic Binaries (Taylor et al. 2003) after observations from the thesis project of the primary author highlighted these as prime

test cases for this method. Twenty other single- and double-lined spectroscopic binaries with separations in and around the predicted range of this experiment were also observed. These three systems consistently displayed a secondary fringe packet and were selected for more detailed monitoring. Data collected on these objects provide additional and predictable positions on the orbits of χ Draconis and HD 184467, and a completely new visual orbit for HD 198084.

7.1. Observational Overview

Data were routinely taken on the CHARA Array's longest baselines (S1-E1 and W1-S1) and other intermediate baselines when the preferred telescopes were assigned to other simultaneous observing experiments. A list of observations for χ Draconis, HD 184467, and HD 198084 along with baselines used is given in Table 1. All observations were taken with the CHARA Classic IR pupil-plane beam combiner through the K' filter as described by ten Brummelaar et al. (2005). The timespan between observing sessions ranged from as little as a week to as long as 260 days. Orbits for these systems were determined with the grid search algorithm (Hartkopf et al. 1989) used by USNO with all available CHARA and speckle interferometry points. Because the systems reported here had spectroscopic orbits, initial values for the search were applied from those solutions. Tables 2 and 3 compare previous orbital elements for χ Draconis and HD 184467 with the ones derived here, Table 4 shows the visual and combined visual–spectroscopic fits for HD 198084, and Table 5 lists the orbital parallaxes and masses calculated from all three systems.

7.2. χ Draconis and HD 184467

In order to ensure that the method of extracting position angles and separations matches with the correct positions on the sky, it is prudent to first employ this technique on systems with well-known spectroscopic and astrometric orbits. Several such systems were observed during the observing runs for this purpose; the results of those observations generally match the predicted positions of the secondary. Two good examples of such test objects are χ Draconis and HD 184467, where multiple speckle observations along with years of spectroscopic orbit data provide a solid template for predictions of the secondary's location.

7.2.1. χ Draconis

HD 170153 ((LAB 5) SB2 (F8IV-V + late-G/early-K dwarf) with visual orbit, $m_v = 3.57$, $\pi = 124.11$ mas, $P \sim 281$ days) is a member of both the Duquennoy & Mayor (1991) sample and the CHARA Spectroscopic Binary catalog with a very wide 127 mas semi-major axis that produces double fringe packets. As this system is very close (8 pc), the primary is sufficiently large in diameter to be resolved at the longest baseline, and thus the lower amplitude fringe packet was determined to be that of the primary star. Hence, vector separations were measured in the opposite direction. With that in mind, the data were reduced and fit remarkably well to the previous spectroscopic–visual orbit from Pourbaix (2000). As this was a test system with a well-known speckle orbit, at first we did not recalculate the orbit in order to see how well the SFP measurements would fit on an established orbit. If one compares the previous speckle measurements with the CHARA SFP measurements shown in the orbit plot in Figure 3, it can be seen that the accuracy of the secondary locations obtained using our SFP measurements is superior to

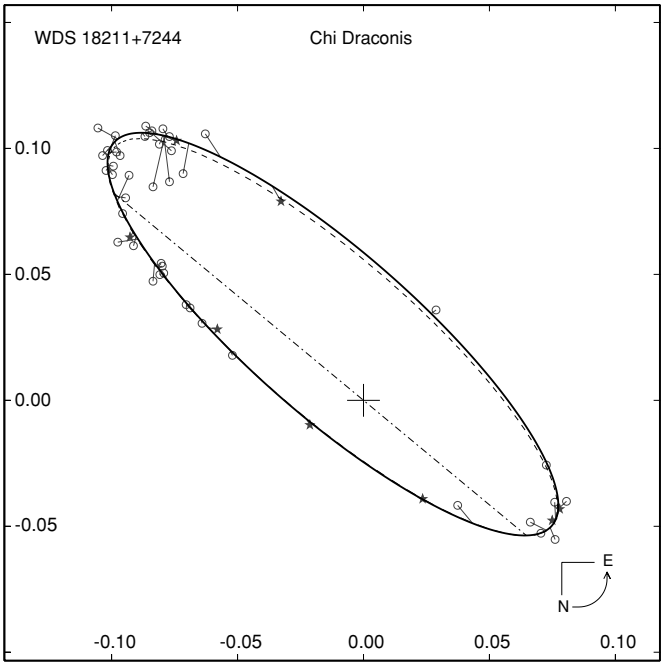

Figure 3. Orbit plot for χ Draconis. The figure shows the relative visual orbit of the system; the x and y scales are in arcseconds. The solid curve represents the orbit determined in this paper with the dashed curve denoting the orbit of Pourbaix (2000). The dot-dashed line indicates the line of nodes. Speckle interferometry measures are shown as open circles. The CHARA Array measures are indicated with a filled star. All measurements are connected to their predicted positions on the orbit by "O−C" lines. The direction of motion is indicated on the northeast orientation in the lower right of the plot.

that of the speckle measurements but require much more effort to obtain. With the inclusion of a few measurements in phases of the orbit that are inaccessible to speckle interferometry around periastron, we recalculated the orbit to see what effect they have on the orbital elements. The obtained orbit, listed in Table 2, and shown in Figure 3 shows very little difference from the previous elements but is based on data obtained over nearly twice as many orbits and produces slightly better errors in some cases.

It can be further noted that every classification of this system has designated the spectral type of the primary as F6-8V/var, the masses calculated for this project as well as all previous determinations seem too small to support this. Using the orbital elements calculated here and the most recent mass ratio calculated from Nordström et al. (2004), we obtain masses of $M_P = 0.96 \pm 0.03\ M_\odot$ and $M_S = 0.75 \pm 0.03\ M_\odot$ which fall below expected ranges for even the latest F-stars. Further investigation of the system is being explored with expanded techniques to get individual radii for the components and confirmation of the probable partial evolution of the primary to subgiant luminosity class.

7.2.2. HD 184467

HD 184467, ((McA 56) SB2 (K2V + K4V?) with visual orbit, $m_v = 6.59$, $\pi = 59.84$ mas, $P \sim 494$ days) a nearby high proper motion star, was an International Astronomical Union (IAU) velocity standard star until McClure (1983) found radial velocity variations and determined the star to be a spectroscopic binary that was double-lined for less than 20% of its orbit. The star was first visually resolved by McAlister et al. (1983) and has since been measured on 32 separate occasions (*The Washington Double Star Catalog*; Mason et al. 2001). Two separate efforts (Arenou et al. 2000; Pourbaix

Table 1
Secondary Locations for SFP Systems χ Draconis, HD 184467, and HD 198084

System	Set	MJD	B (m)	$\vec{\theta}$ (deg)	$\vec{\rho}$ (mas)	BY_{calc}	θ	ρ (mas)
χ Dra	1	53891.303	257.88	340.94	19.89			
		53891.446	236.41	117.32	43.42			
		53891.497	222.06	100.73	65.23			
		53892.446	280.11	10.21	60.77	2006.4272	57.4	88.8
	2	53996.196	281.17	0.79	79.47			
		53996.282	275.71	156.97	59.98	2006.7135	22.4	85.5
	3	54314.317	281.08	3.05	107.61			
		54314.321	281.14	1.91	108.08			
		54314.419	274.55	154.65	61.09			
		54315.290	280.17	9.92	112.12			
		54315.385	278.38	163.49	77.81	2007.5855	215.6	127.0
	4	54376.116	236.98	298.06	50.76			
		54376.168	222.50	281.21	77.85	2007.7536	234.9	113.1
	5	54956.264	258.01	18.40	45.62			
		54956.268	258.28	17.01	45.19			
		54956.349	259.57	172.68	16.35			
		54956.360	289.37	116.56	40.58			
		54956.374	249.15	55.37	64.21			
		54956.442	252.49	143.92	8.36			
		54956.459	271.33	30.83	52.46	2009.3407	243.9	64.5
	6	54970.276	226.58	73.01	20.95			
		54970.285	230.27	70.32	14.12			
		54970.296	234.78	66.95	13.57			
		54970.321	289.18	116.90	21.88			
		54970.345	293.83	108.45	23.03			
		54970.354	295.66	105.04	23.49			
		54970.362	297.21	102.09	23.36			
		54970.370	298.69	99.20	23.25			
		54970.380	255.36	331.57	17.55			
		54970.388	254.42	148.81	19.35			
		54970.413	251.45	141.54	18.88	2009.3789	294.5	23.42
	7	54984.297	258.65	345.09	32.28			
		54984.308	252.63	232.26	42.79			
		54984.321	296.65	283.15	13.63	2009.4174	30.78	45.64
	8	55018.199	247.49	56.80	90.28			
		55018.209	250.79	53.93	88.36			
		55018.248	262.12	42.75	83.70			
		55018.500	313.14	189.81	56.54	2009.5104	60.83	89.04
HD 184467	1	53647.169	251.09	122.31	38.13			
		53647.173	249.95	121.44	38.95			
		53647.176	248.57	120.42	37.24			
		53654.159	314.73	186.15	30.22			
		53654.162	314.84	185.36	29.91			
		53654.166	314.93	184.59	30.68	2005.7662	153.5	54.4
	2	53889.388	295.80	36.77	69.37			
		53889.461	310.54	19.37	59.88			
		53890.280	276.43	3.28	55.81			
		53891.324	276.11	349.98	42.01			
		53891.507	248.82	120.60	19.07			
		53892.458	311.19	18.05	59.87	2006.4236	45.9	101.3
	3	53990.155	268.78	322.09	38.56			
		53990.229	251.45	302.60	31.18			
		53996.212	314.25	8.87	40.15			
		53996.292	313.72	348.91	41.85	2006.7048	352.8	63.4
	4	54247.376	241.68	35.25	52.47			
		54247.480	258.23	11.65	17.64			
		54248.436	270.22	144.93	45.43			
		54249.437	254.45	20.45	32.19			
		54249.440	254.92	19.61	30.54			
		54249.486	258.91	9.09	16.06			
		54249.493	259.27	7.31	15.12	2007.4049	88.5	105.5

Table 1
(Continued)

System	Set	MJD	B (m)	$\vec{\theta}$ (deg)	$\vec{\rho}$ (mas)	BY_{calc}	θ	ρ (mas)
	5	54272.409	310.09	20.24	37.56			
		54272.413	310.54	19.38	35.28			
		54272.481	315.09	2.64	15.42			
		54273.314	274.89	160.01	15.95	2007.4703	80.6	112.5
HD 198084	1	53889.412	288.97	222.65	21.27			
		53889.472	305.81	208.95	14.85			
		53890.436	289.91	274.22	14.60			
		53892.397	286.09	224.36	22.53			
		53892.436	299.27	215.32	17.71			
		53892.481	308.97	204.94	12.12	2006.4260	91.9	32.4
	2	53988.375	210.31	279.53	24.55			
		53989.249	262.20	311.72	58.08			
		53989.328	234.71	291.56	38.43			
		53989.372	210.46	279.60	23.96			
		53990.138	275.71	340.78	72.17			
		53990.144	275.43	339.13	73.19			
		53990.218	267.92	319.12	64.49			
		53990.352	220.94	284.50	29.82	2006.6965	171.0	75.3
	3	54249.418	242.69	35.70	68.76			
		54249.422	243.76	34.83	68.55			
		54249.474	254.28	23.52	58.41			
		54249.481	255.33	21.91	58.16	2007.4039	246.1	80.4
	4	54254.388	168.62	2.79	28.40			
		54254.425	168.42	173.90	15.50			
		54255.388	101.78	134.14	37.15			
		54255.436	105.56	118.12	56.00			
		54255.485	107.76	102.73	63.80	2007.4211	252.0	77.5
	5	54268.458	241.22	135.19	37.21			
		54269.497	314.87	256.93	34.22			
		54272.472	313.25	252.64	37.77			
		54273.321	276.83	277.73	17.70	2007.4592	254.1	74.4
	6	54307.319	303.90	239.04	29.02			
		54307.423	248.38	150.11	53.80			
		54307.430	245.92	151.78	55.01			
		54309.494	314.92	103.02	22.85	2007.5659	274.2	62.1
	7	54314.397	316.20	7.74	12.05			
		54314.481	314.92	167.02	20.52			
		54315.347	312.39	19.24	10.21			
		54315.430	316.87	178.88	12.97			
		54315.474	315.22	168.04	20.81			
		54315.514	311.13	158.41	30.33	2007.5859	279.5	57.6
	8	54359.261	255.37	125.24	40.47			
		54359.407	308.98	335.07	40.05	2007.7067	320.0	41.4
	9	54375.119	273.53	331.24	30.66			
		54376.145	270.37	143.42	29.92			
		54376.194	261.26	310.71	25.52			
		54376.291	223.03	105.52	17.57			
		54376.313	210.45	99.60	16.42	2007.7529	337.7	29.8
	10	54423.155	233.97	350.10	17.31			
		54423.179	232.44	344.40	24.07			
		54424.184	231.80	342.61	25.80	2007.8862	113.4	39.3
	11	54632.455	153.71	204.07	57.60			
		54632.508	156.21	219.44	82.61			
		54633.440	196.89	286.75	67.29	2008.4554	206.0	91.5
	12	54693.343	256.52	143.78	13.47			
		54693.382	242.62	153.83	24.75			
		54693.463	313.15	287.64	44.66			
		54693.499	307.82	296.49	31.29	2008.6212	222.8	89.7
	13	54759.098	307.17	242.73	62.11			
		54759.107	268.84	129.48	16.01			
		54759.239	225.06	163.53	56.90			

Table 1
(Continued)

System	Set	MJD	B (m)	$\vec{\theta}$ (deg)	$\vec{\rho}$ (mas)	BY_{calc}	θ	ρ (mas)
		54759.247	315.99	278.89	27.00			
		54759.301	310.85	292.11	12.08	2008.8015	241.1	79.5
	14	54956.418	254.02	28.42	21.20			
		54956.429	277.00	324.91	43.56			
		54956.494	275.65	271.34	22.24			
		54956.504	293.31	289.50	32.77			
		54956.510	295.87	353.95	37.31	2009.3415	121.0	42.7
	15	54970.426	276.61	281.32	41.66			
		54970.437	282.37	345.44	40.24			
		54970.441	283.48	346.21	40.87			
		54970.479	274.28	296.18	47.63	2009.3798	136.0	50.2
	16	54984.334	250.53	322.21	53.01			
		54984.342	254.38	325.26	53.07			
		54984.351	258.45	328.22	48.76	2009.4179	160.9	65.3
	17	55018.272	266.63	216.30	25.21			
		55018.281	271.55	218.41	26.83			
		55018.292	276.57	220.74	29.24			
		55018.307	280.71	222.72	32.92			
		55018.442	313.51	206.78	14.44			
		55018.454	313.35	210.65	19.58			
		55018.465	312.94	213.62	21.76			
		55019.436	260.27	320.36	58.45			
		55019.449	256.75	323.68	55.90	2009.5119	165.5	70.9

Notes. Observation log for χ Draconis, HD 184467, and HD 198084 on the CHARA Array from 2005–2009. Each set of vector observations (along with the projected baseline length and epoch of observation) in Columns 2 through 5 were combined to create the true location of the secondary and average time of all the data points defined in the last three columns. Errors associated with each observation for χ Draconis and HD 184467 are $\leqslant$1 mas and 1–4 mas for HD 198084.

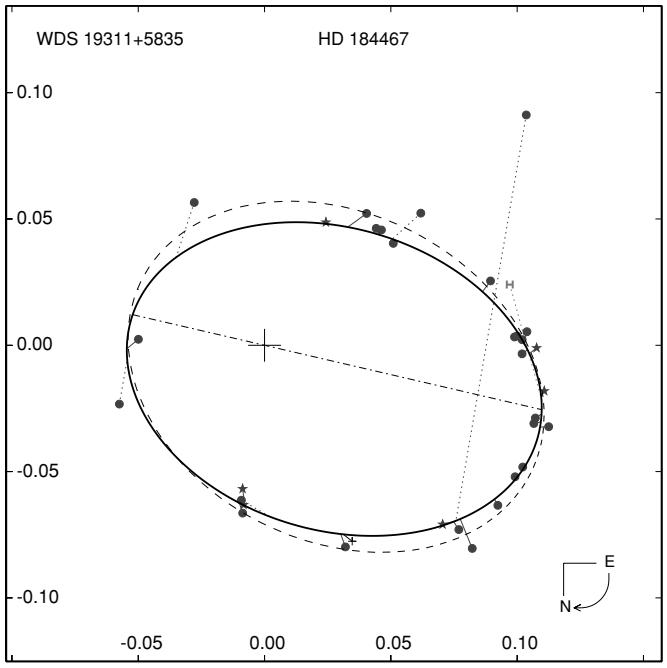

Figure 4. Orbit plot for HD 184467. Included in this solution are all speckle interferometry measurements from the Fourth Catalog of Interferometric Measurements of Binary Stars (Hartkopf et al. 2001) in addition to the CHARA SFP Survey data. The filled circles represent the speckle measurements from the Fourth Catalog, the *Hipparcos* measurement is denoted by the H, and the CHARA measurements are represented by the stars. The orbit calculated with the inclusion of the CHARA points is the solid black line which is similar to the orbit of Pourbaix shown by the dashed oval. The odd data point 1984.7780 given zero weight.

Table 2
χ Draconis Orbital Elements

Elements	Pourbaix (2000)	This Paper
P (days)	280.560 ± 0.0621	280.528 ± 0.02228
P (yr)	0.76815 ± 0.00017	0.7680599 ± 0.000061
T_0 (MJD)	46005.63 ± 0.548	46004.68 ± 0.949
T_0 (BY)	1984.83499 ± 0.00150	1984.83239 ± 0.00259
a″	0.1230 ± 0.0012	0.1244 ± 0.0011
e	0.414 ± 0.008	0.428 ± 0.012
i (°)	74.8 ± 0.79	74.42 ± 0.58
ω (°)	299.9 ± 0.97	119.3 ± 1.1
Ω (°)	50.5 ± 0.60	230.30 ± 0.51

Notes. Our elements are, with the exception of eccentricity, all within 1σ of that of Pourbaix, although several of our errors are smaller. Pourbaix's orbit covered 28 revolutions and was based on 18 speckle points whereas this effort's orbit covers 47 revolutions and includes 29 points; it is believed that the period error is justifiable.

2000) combined spectroscopy with speckle observations from the *Fourth Catalog of Interferometric Measurements of Binary Stars* (Hartkopf et al. 2001) and determined the complete set of orbital elements. The data collected at the CHARA Array provide six new points that have been incorporated with the existing high-resolution observations. A recalculation of the orbit with the SFP measurements included provides a third complete orbital solution and is listed in Table 3 along with the two previous combined visual–spectroscopic solutions. The differences between the three solutions are minor and generally within the previous errors and the reduced χ^2 calculated for the orbit remains small (1.28). The relative orbits are shown in Figure 4.

Table 3
Orbital Solutions for HD 184467

Elements	Pourbaix (2000)	Arenou et al. (2000)	This Paper
P (days)	494.091 ± 0.26	494.75 ± 0.48	494.16 ± 0.58
P (yr)	1.352776 ± 0.00071	1.35458 ± 0.00131	1.35297 ± 0.00159
T_0 (MJD)	46164.9 ± 1.66	48641.21 ± 3.1	46671.4 ± 8.5
T_0 (BY)	1985.2711 ± 0.00454	1992.0509 ± 0.008488	1986.6579 ± 0.02332
a''	0.0860 ± 0.0014	0.084 ± 0.003	0.08420 ± 0.00084
e	0.3600 ± 0.0078	0.340 ± 0.013	0.371 ± 0.006
i (°)	144 ± 2.4	144.6 ± 1.7	144.0 ± 1.29
ω (°)	356 ± 2.1	177.8 ± 2.1	16.57 ± 4.1
Ω (°)	243 ± 1.5	74.6 ± 6.8	256.9 ± 2.66

Note. Comparison of two previous visual and spectroscopic orbital solutions for HD 184467 with the new calculation from CHARA data.

Table 4
Orbital Solutions for HD 198084

Elements	Orbgrid (WIH)	Vis-Spec (TOKO)
P (days)	522.596 ± 0.591	523.4192 ± 0.1010
P (yr)	1.430822 ± 0.00162	1.4331 ± 0.0003
T_0 (MJD)	50212.861 ± 0.592	50206.004 ± 0.609
T_0 (BY)	1996.35400 ± 0.01167	1996.335 ± 0.0017
a''	0.0656 ± 0.0021	0.065 ± 0.001
e	0.556 ± 0.005	0.551 ± 0.004
i (°)	27.4 ± 1.7	24.53 ± 3.13
ω (°)	257.4 ± 3.4	68.86 ± 0.76
Ω (°)	136.8 ± 3.6	325.21 ± 1.05

Notes. Preliminary orbital elements for HD 198084. While the orbit from Orbgrid (Hartkopf et al. 1989) in the first column fits with the previous spectroscopic elements, the inclination is higher than the value of 23°±1° predicted by Griffin (1999). The second orbital solution is a combined visual–spectroscopic fit determined by the ORBIT program by Andrei Tokovinin (1993).

Table 5
Masses and Orbital Parallax for χ Draconis, HD 184467, and HD 198084

Elements	χ Draconis	HD 184467	HD 198084
π_{orb} (mas)	123.4 ± 1.9	59.2 ± 2.04	39.8 ± 4.8
M_P ($M_\odot$)	0.96 ± 0.03	0.82 ± 0.09	1.071 ± 0.037
M_S ($M_\odot$)	0.75 ± 0.03	0.77 ± 0.09	1.047 ± 0.037

7.3. SFP Orbital Solution for HD 198084

HD 198084 (SB2 (F8IV-V + F9IV-V), $m_v = 4.51$, $\pi = 36.64$, $P \sim 523.8$ days) has a long history of radial velocity measurements, culminating with the determination of a 523 day radial velocity variation (Griffin 1999). He noted that earlier investigators Abt & Levy (1976) and Beavers & Eitter (1986) had not detected the companion's spectrum even at favorable phases. His effort was more successful, catching a conspicuous double-lined phases on 24 out of 38 epochs between 1996 and 2000. Using all previous data available to him, Griffin determined an orbit with residuals of ±0.4 km s^{-1} and inferred from the commonly accepted spectral typing that an inclination of approximately 23° ± 1° would be necessary for the masses to fall within the appropriate range for stars of this spectral type. Furthermore, he pointed out that the star is a good target for speckle interferometry due to its brightness and a separation likely larger than 50 mas. Nevertheless, it appears that only three speckle measurements of HD 198084 have been taken and though it should have been resolved, the companion was not detected even with predicted separations of 91 and 92 mas.

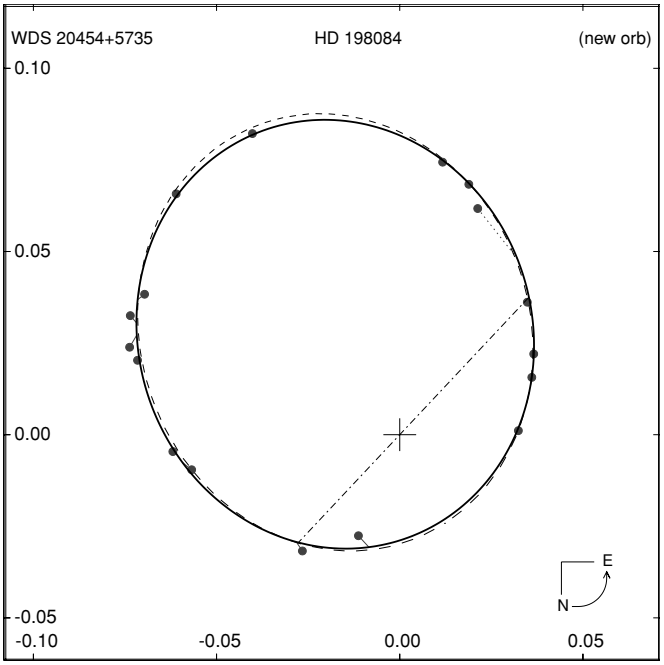

Figure 5. Orbit plot for HD 198084, 2005–2009. Combined visual–spectroscopic solution (Tokovinin 1992, 1993; solid line) using all available data which is consistent with both the visual only solutions of Orbgrid (Hartkopf et al. 1989; dashed line) as well as the spectroscopic solution of Griffin (1999). The orbit is configured in the same manner as Figure 3.

SFPs for this star were detected on both baselines early in this program, and because it was previously unresolved, HD 198084 was observed as frequently as possible. Hence, a total of 60 observations were made over seven separate observing runs to produce 17 individual astrometric points for this orbit. The system was observed within 15 days of periastron on two separate occasions, and, due to the eccentric nature of this orbit and the rapid movement of the secondary, the observations during those two observing runs produced three points for the orbit.

Our new astrometric measurements were combined with the spectroscopic elements of Griffin (1999) in a grid search to determine the previously unknown visual elements of the system. We have sampled two orbital revolutions to date, and Figure 5 shows that it provides a reasonably good distribution of observed phases, including observations before and after periastron. Calculated orbital elements with errors are listed in Table 4 and the orbital parallax and mass comparisons in Table 5. The masses obtained from the orbit determined here and from

the $M \sin^3 i$ values given by the spectroscopic orbit of Griffin are $M_P = 0.791 \pm 0.289\ M_\odot$ and $M_S = 0.771 \pm 0.288\ M_\odot$.

Additionally, a simultaneous solution utilizing all the radial velocity and visual/speckle data was carried out with an interactive program developed by Andrei Tokovinin (1992, 1993) that computes all ten orbital elements. This technique employs the method of least squares to yield elements satisfying both radial velocity and astrometric measurements as described in McAlister et al. (1995). This solution is consistent with interferometric only determinations using Orbgrid (Hartkopf et al. 1989). The solutions for the combined visual/spectroscopic solution are listed in Tables 4 and 5 which produce masses ($M_P = 1.071 \pm 0.037\ M_\odot$ and $M_S = 1.047 \pm 0.037\ M_\odot$) that are comparable to the Orbgrid solution and are more realistic for stars of the expected spectral type.

From these data, we have also calculated the orbital parallax determined from this orbit. Previous determinations from *Hipparcos* give the parallax as 36.87 ± 0.46 mas (Perryman et al. 1997) and more recently updated in 2008 as 36.64 ± 0.46 mas (van Leeuwen 2008). G. Torres (2008, private communication) recalculated the *Hipparcos* parallax with the CHARA visible orbit and determined the revised distance of 36.26 ± 0.36 mas. From the inclination of 24°.5 ± 3°.1 calculated from the preliminary orbit, the orbital parallax is determined to be 39.8 ± 4.8 mas. Griffin (1999) postulated that the parallax was not entirely reliable as it does not take into account the orbit, but the orbital parallax calculated here seems to fall within the expected range.

With the addition of observations from 2009 and a new error analysis for the complete data set, the orbital solutions are more consistently aligned with the previous predictions for the system, albeit with larger than desired mass errors. While the sampling of the orbit is not unreasonable for determining an orbit solution, the absence of additional observations at apastron makes this solution somewhat preliminary in nature.

8. CONCLUSION AND DISCUSSION

For the three systems that this project followed through the development of the current SFP process, the orbital solutions and masses determined here seem quite promising. The continuation of this process opens up hundreds of spectroscopic binary systems for observation where the components were either never far enough apart to be resolved by speckle interferometry or were too close in phases of the orbit that are important for quality determinations of their orbital elements. As with other techniques, it is possible with time and patience to produce complete orbits of binary systems entirely with this method even though it is cumbersome. While refining this technique and upgrading the instruments of the CHARA Array, possibilities for further improving the data quality have produced some parallel methods which further enhance the scientific output of such a simple method.

The main difficulty of using the SFP technique is that we are only able to use one baseline of the CHARA Array at a time with the current beam combiners. A small but significant amount of time is lost switching between baselines, configuring the delay lines, and resetting the computer systems between each observation. While this has been reduced to as little as 5 minutes with proper planning, it is far from ideal and would benefit from a multiple beam combiner. Fortunately, SFP measurements are being adapted currently for the CHARA Array's newest beam combiner, CLassic Interferometry on Multiple Baselines (CLIMB; ten Brummelaar et al. 2008). The advent of the CLIMB instrument will enable us to measure SFPs on three separate baselines simultaneously, producing an astrometric measurement of the binary system in one-third the time. After the testing phase of the CLIMB combiner, the current CHARA Classic combiner will undergo a refit to accommodate a third beam as well and could provide an avenue for six simultaneous baseline measurements for increased accuracy as well as faster radii measurements.

This does not make obsolete the single baseline measurements of the current SFP technique. For many binary systems, it is still acceptable to collect data on one baseline at a time before switching to a separate baseline to get a reliable position for the secondary star. It does allow extra flexibility based on how many and which telescopes are available at any given time to produce measurements of binary stars and their orbits. The orbits and measurements of the systems herein are the first test cases for the method which will be followed by many targets that are currently being observed whose orbits are incomplete, need to be improved, or are nonexistent. Furthermore, this technique provides an excellent observational tool to bridge the gap between classical and speckle interferometry and adding a significant number of spectroscopic binaries to be observed for direct measurements of their fundamental properties.

The CHARA Array, operated by Georgia State University, was built with funding provided by the National Science Foundation, Georgia State University, the W. M. Keck Foundation, and the David and Lucile Packard Foundation. This research is supported by the National Science Foundation under grant AST 0908253 as well as by funding from the office of the Dean of the College of Arts and Science at Georgia State University. B.D.M. and W.I.H. have been supported by the National Aeronautics and Space Administration under reimbursable no. NNH06AD70I, issued through the Terrestrial Planet Finder Foundation Science program. This research has made use of the SIMBAD database, operated at CDS, Strasbourg, France. Thanks are also extended to Ken Johnston and the U. S. Naval Observatory for their continued support of the Double Star Program. We thank John Monnier and Guillermo Torres for the orbital solutions and distance corrections they provided.

REFERENCES

Abt, H. A., & Levy, S. G. 1976, ApJS, 30, 273
Arenou, F., Halbwachs, J. L., Mayor, M., Palasi, J., & Udry, S. 2000, in IAU Symp. 200, Birth and Evolution of Binary Stars, ed. B. Reipurth & H. Zinnecker (Cambridge: Cambridge Univ. Press), 135
Bagnuolo, W. G., Jr., et al. 2006, AJ, 131, 2695
Beavers, W. I., & Eitter, J. J. 1986, ApJS, 62, 147
Boden, A. F., et al. 1999, ApJ, 527, 360
Bracewell, R. N. 2000, The Fourier Transforms and Its Applications, 3rd ed. (Colombus, OH: McGraw Hill)
Duquennoy, A., & Mayor, M. 1991, A&A, 248, 2
Dyck, H. M. 2000, in Principles of Long Baseline Stellar Interferometry, ed. P. R. Lawson (JPL PUB 00-009; Pasadena, CA: NASA), 185
Dyck, H. M., Benson, J. A., & Schloerb, F. P. 1995, AJ, 110, 1433
Franz, O. G., Wasserman, L. H., Nelan, E., Lattanzi, M. G., Bucciarelli, B., & Taff, L. G. 1992, AJ, 103, 190
Griffin, R. F. 1999, Observatory, 119, 272
Hartkopf, W. I., McAlister, H. A., & Franz, O. G. 1989, AJ, 98, 1014
Hartkopf, W. I., Mason, B. D., Wycoff, G. L., & McAlister, H. A. 2001, Fourth Catalog of Interferometric Measurements of Binary Stars, http://ad.usno.navy.mil/wds/int4.html
Lane, B. F., & Muterspaugh, M. W. 2004, ApJ, 601, 1129
Mason, B. D., Wycoff, G. L., Hartkopf, W. I., Douglass, G. G., & Worley, C. E. 2001, AJ, 122, 3466
McAlister, H. A., Hartkopf, W. I., Hendry, E. M., Campbell, B. G., & Fekel, F. C. 1983, ApJS, 51, 309

McAlister, H. A., Hartkopf, W. I., Mason, B. D., Fekel, F. C., Ianna, P. A., Tokovinin, A. A., Griffin, R. F., & Culver, R. B. 1995, AJ, 110, 366
McClure, R. D. 1983, PASP, 95, 201
Nordström, B., et al. 2004, A&A, 418, 989
Perryman, M. A. C., et al. 1997, A&A, 323, L49
Pourbaix, D. 2000, A&AS, 145, 215
Schloerb, F. P. 1990, Proc. SPIE, 1237, 154
Shao, M., & Colavita, M. M. 1992, A&A, 262, 353
Taylor, S. F., McAlister, H. A., & Harvin, J. A. 2003, PASP, 115, 609
ten Brummelaar, T. A., et al. 2005, ApJ, 628, 453
ten Brummelaar, T. A., et al. 2008, Proc. SPIE, 7013, 701308-12
Tokovinin, A. A. 1992, in ASP Conf. Ser. 32, IAU Coll. 135, Complementary Approaches to Double and Multiple Star Research, ed. H. A. McAlister & W. I. Hartkopf (San Francisco, CA: ASP), 573
Tokovinin, A. A. 1993, Astron. Lett., 19, 73
van Leeuwen, F. 2008, *Hipparcos*, the New Reduction, VizieR Online Data Catalog, 1311